Nat. Hazards Earth Syst. Sci. Discuss., https://doi.org/10.5194/nhess-2017-428
Manuscript under review for journal Nat. Hazards Earth Syst. Sci.
Discussion started: 19 December 2017

Natural Hazards and Earth System Sciences
Discussions

Adopting I_3–R_{24} rainfall index and landslide susceptibility on the establishment of early warning model for rainfall-induced shallow landslides

Lun-Wei Wei[1,2], Chuen-Ming Huang[1,3], Chyi-Tyi Lee[3], Chun-Chi Chi[4], and Chen-Lung Chiu[4]

[1]Disaster Prevention Technology Research Center, Sinotech Engineering Consultants, INC., Taiwan
[2]Department of Geosciences, National Taiwan University, Taiwan
[3]Institute of Applied Geology, National Central University, Taiwan
[4]Central Geological Survey, MOEA, Taiwan

Correspondence to: Lun-Wei Wei (d03224007@ntu.edu.tw)

Abstract. Rainfall-induced landslide is one of the most devastating natural hazards in the world and the setup of early warning models is a pressing need for reducing losses and fatalities. Most part of landslide early warnings are based on rainfall thresholds defined at the regional scale, regardless of the different landslide susceptibility of each slope. Here we tried to divide slope units in southern Taiwan into three categories (high, moderate, low) according to their susceptibility. For each category, we established their rainfall thresholds separately so as to provide differentiated thresholds for different susceptibility. Logistic regression (LR) analysis was performed to evaluate the landslide susceptibility by using event based landslide inventories and predisposing factors. Through the analysis of rainfall patterns of more than 900 landslide cases gathered from field investigation, 3-hour mean rainfall intensity (I_3) was recognized as a key rainfall index for short duration but high intensity rainfall; on the other hand, 24-hour accumulated rainfall (R_{24}) was recognized as a key rainfall index for long duration but low intensity rainfall. Thus, the I_3–R_{24} rainfall index was used for the establishment of rainfall thresholds in this study. Finally, an early warning model was proposed by setting warning signs including yellow (advisory), orange (watch) and red (warning) according to the concept of hazard matrix. These differentiated thresholds and warning signs can provide essential information for local government on evacuating decision of residents.

Keywords: rainfall-induced landslide, landslide susceptibility analysis, rainfall threshold, early warning

1 Introduction

Rainfall-induced landslide is one of the most perilous natural hazards, causing severe casualties and economic losses all over the world (Ayalew, 1999; Evans et al., 2007; Tsou et al., 2011、Petley, 2012; Wang et al., 2015; Iverson et al., 2015; Sassa et al., 2015; Fan et al., 2017). Therefore, many efforts have been made to evaluate the susceptibility and set criteria of issuing early warning for the sake of saving lives and properties.

Landslide could be triggered by either rainfall or earthquake in Taiwan (Lee et al., 2004), especially the former. Taiwan was invaded by several typhoons which brought great amounts of rainfall every year. Therefore, recognizing the area that might have potential rainfall-induced landslide was important and landslide susceptibility analysis was a general method. We adopted a statistical susceptibility model in this study based on the assumption that the factors which caused slope-failure in a region were the same as those which will generate landslides in the future (Guzzetti et al., 1999). There were several statistical models that have been proposed and widely utilized in landslide susceptibility in recent years, especially logistic regression (Guzzetti et al., 1999; Lee et al., 2004, 2008a, 2008b, 2014). Therefore, we applied logistic regression (LR) in this study.

Nat. Hazards Earth Syst. Sci. Discuss., https://doi.org/10.5194/nhess-2017-428
Manuscript under review for journal Nat. Hazards Earth Syst. Sci.
Discussion started: 19 December 2017

Natural Hazards and Earth System Sciences
Discussions

On the other hand, rainfall thresholds for landslides can be categorized as statistical approaches and deterministic approaches. In the former method, thresholds are decided by collecting historical landslide cases and analyzing their rainfall parameters as well as probability lines of rainfall conditions (Caine, 1980; Guzzetti et al., 2008). In the latter method, thresholds are decided by calculating safety factors of each slope or grid with geomaterial and rainfall parameters (Terlien, 1998; Kim et al., 2010).

Statistical rainfall thresholds for shallow landslide have been well discussed (Guzzetti et al., 2007). They can mainly classify into 5 categories including intensity-duration (Brunetti et al., 2010; Zhou et al., 2014; Pradhan et al., 2017), accumulated rainfall-duration (Martelloni, 2011; Vessia et al., 2014; Gariano et al., 2015; Rossi et al., 2017), accumulated rainfall (Corominas and Moya, 1999; Bell and Maud, 2000), intensity-accumulated rainfall (Hong et al., 2005) and accumulated rainfall-accumulated rainfall (Osanai et al., 2010; Turkington et al., 2014).

Most of the studies mentioned above set up only one threshold for their study area in spite of the difference in physical settings (geology, geomorphology, meteorological condition) of that region. Recently, some studies subdivided their study area into several homogeneous sub-zones in order to discuss the influence of physical settings on thresholds (Hong and Adler, 2008; Segoni et al., 2014; Lee et al., 2015; ~~Segoni et al., 2015~~; Rosi et al., 2015; Peruccacci et al., 2017). However, for a smaller area like slope units, the difference in susceptibility may lead to a different warning threshold, e.g., for a high susceptibility slope, its warning threshold may be probably lower than a low susceptibility slope. In order to address this gap in knowledge, we tried to divide slope units into three different landslide susceptibility levels (high, moderate, low) and established their rainfall thresholds separately. Besides, we set warning signs by adopting the concept of hazard matrix and examine if differentiated warning thresholds for different susceptibility existed.

2 Study area

Taiwan is located at the western Pacific Ocean, on the convergent plate boundary zone of Philippine Sea plate and Eurasian plate. The orogenic uplift rate is 5 ~ 7 mm/yr (Willett et al., 2003), however, the exhumation rate is also as high as 3 ~ 6 mm/year (Dadson et al., 2003) due to the fractured geological materials and the high mean annual precipitation up to 2,500 ~ 3,000 mm brought by typhoons and monsoons every year (Hsu, 2013). The frequent nature disasters and high population density (23 million people over 36,000 km^2) make Taiwan one of the countries most exposed to multiple hazards (Dilley et al., 2005).

The study area is located in southern Taiwan (red box in Fig. 1), including the region of 47 1:25,000 scale maps (about 7,258.5 km^2) and covering densely inhabited as well as landslide threatening hillslopes. The elevation ranges from 3,243 meters in mountain area to 0 meters in plain area while the gradient ranges from 87° to 0°. Geological settings are mainly sedimentary rocks composed of sandstone, shale, mudstone and conglomerate in the Western Foothills as well as metamorphic rocks composed of slate, argillite and metasandstone in Central Range.

Nat. Hazards Earth Syst. Sci. Discuss., https://doi.org/10.5194/nhess-2017-428
Manuscript under review for journal Nat. Hazards Earth Syst. Sci.
Discussion started: 19 December 2017

Natural Hazards and Earth System Sciences
Discussions

3 Data and methodology

3.1 Data

3.1.1 Landslide inventory

Landslide inventory is essential for the assessment of landslide susceptibility or spatio-temporal changes (Van Westen et al., 2003; Guzzetti et al., 2012; Samia et al., 2017; Valenzuela et al., 2017). In this study, there were four procedures for the construction of landslide inventories. Firstly, the landslide inventories (Table 1) were interpreted manually from SPOT 5 image. Secondly, the aerial photograph and google earth were applied to check the locational correctness of inventories and confirm the type of landslides. This study used only shallow landslides to analyze and the other types (e.g. rockfall) were filtered. Thirdly, we selected landslides form inventories randomly to verify the correctness of location and boundary via fieldwork. Finally, event-based triggered landslides, including new-generated landslide and expanded landslide due to the event, were identified through the comparison of inventories before and after each rainfall event. In this study, there were six events of triggered landslide inventories were built.

3.1.2 Landslide occurrence time and field investigation

Rainfall conditions such as intensity, duration, accumulated rainfall that induced landslides are key data while applying the statistical method to establish the rainfall thresholds for landslides (Guzzetti et al., 2007, 2008; Brunetti et al., 2010; Peruccacci et al., 2017). In order to analyze rainfall conditions for each landslide case used in this study, a flowchart was proposed in this study (Fig. 2). We gathered landslide occurrence time by inquiring residents during field investigation or collecting reports in newspapers. Besides, detailed characteristics of landslides such as lithology, geological structure, joint, strength, area, depth and mechanism were also recorded during field work. Finally, 941 landslide cases including their occurrence time (date and hour) and characteristics of landslides were gathered for further analysis of the rainfall conditions.

3.1.3 Slope unit

This study used slope unit that based on the features of geomorphology such as ridges and river valleys to analyze landslide susceptibility (Carrara, 1988; Carrara et al., 1991, 1995; Guzzetti et al., 1999; Schlögel et al., 2017; Yang, 2017). In order to delineate the boundary correctly, the 5m DEM were acquired from the Department of Interior, Taiwan. However, the DEM was smoothed and reduced to 10m resolution for the sake of reducing noises. Through the mapping concept proposed by Xie et al. (2004), the slope units were mapped automatically and modified manually (Fig. 3). Each slope unit was given a unique code and separated into stable or unstable unit.

3.1.4 Landslide Susceptibility Factors

Many factors could induce landslide, but each factor had different effect. This study initially selected some factors that were suitable to construct landslide susceptibility model for slope units. These factors included rock mass strength-size

Nat. Hazards Earth Syst. Sci. Discuss., https://doi.org/10.5194/nhess-2017-428
Manuscript under review for journal Nat. Hazards Earth Syst. Sci.
Discussion started: 19 December 2017

Natural Hazards and Earth System Sciences
Discussions

classification (RMSSC I~VII), dip slope, average slope, variance of slope, ratio of steep slope, total slope high, average elevation, average curvature, variance of curvature, fault density, fold density, average wetness, rainfall intensity, total rainfall, 3-hour mean rainfall intensity (I_3) and 24-hour accumulated rainfall (R_{24}). They could be analyzed through graphic discrimination that included success rate curve, probability of failure curve and difference between landslide and non-landslide groups (Lee, 2014). Finally, we applied factor correlation analysis and deleted the high relative factors (Table 2).

Lithology was a critical element in slope stability. However, there were more than 50 types of lithology in this study area, which was unfavorable for the analysis. Therefore, the 1:25,000 rock mass strength-size classification (Franklin, 1975) maps from the Central Geological Survey were adopted to replace lithology. Dip slope inventory used in this study was interpreted manually from 1:5,000 aerial photographs. The average slope and the variance of slope was obtained by averaging and calculating standard deviation of all the grid cells in the slope unit separately. The ratio of steep slope was calculated by dividing the area that greater than 30 degrees by total area of slope unit. The average curvature and variance of curvature could also be calculated in GIS software. The fold density was the total length of all the folds divided by the total area in each slope unit. The average wetness was calculated by following the method proposed by Wilson and Gallant (2000). The hourly rainfall records of two typhoon events in this study were collected from Central Weather Bureau, Taiwan. According to these rainfall records, the 3-hour mean rainfall intensity (I_3) and 24-hour accumulated rainfall (R_{24}) in each rainfall station were calculated. Besides, Kriging interpolation method was applied to generate the precipitation distribution map for the whole study area.

3.2 **Methodology**

3.2.1 **Landslide susceptibility analysis**

The main purpose of landslide susceptibility analysis was to determine relative possibility of landslide occurrence. However, the deterministic methods required geotechnical material properties which were difficult to obtain for the regional landslide susceptibility (Montgomery and Dietrich, 1994; Van Westen and Terlien, 1996). The qualitative methods depended on the experience and knowledge of the expert who carried out the analysis. The machine learning methods equired more training time to build model by trial and error (Gorsevski and Jankowski, 2010; Yeon et al., 2010; Yilmaz, 2010; Marjanovic et al., 2011; Lee et al., 2012; Song et al., 2012). In order to avoid these difficulties, this study adopted statistical methods. Besides, due to landslide was a complex phenomenon, a nonlinear analysis was more suitable for this study. Recently, logistic regression (Yilmaz, 2010; Lee et al., 2012; Lee et al., 2014; Lee et al., 2015; Schlögel et al., 2017) and discriminant analysis (Lee et al., 2004, 2008a, 2008b) were often used to analyze landslide susceptibility in the statistical methods, therefore, LR was applied to evaluate the susceptibility of each slope unit (Guzzetti et al., 1999; Ayalew and Yamagishi, 2005). LR function was expressed as follows:

$$P = \frac{1}{1+e^{-z}} \tag{1}$$

$$z = \sum_{i=1}^{m} L_i w_i + \sum_{j=1}^{n} F_j w_{m+j} + C \tag{2}$$

where P was the landslide susceptibility; L was RMSSC factor; F was other factors (Table 2); w was regression coefficient

and *C* was constant. The six event-based triggered landslide inventories in this study were divided into two parts randomly. One was for training model and the other was for the validation. In addition, the non-landslide data were much more than landslide data, so we selected the same amount of non-landslide and landslide data randomly for training in SPSS software. Besides, several sets of randomly selected samples (especially non-landslide data) were also tested for the analysis of landslide susceptibility in order to ensure the model were stable enough, not variating with alternating samples. Finally, the distribution of the failure ratio and landslide susceptibility in each slope unit was plotted and then used in classifying landslide susceptibility level (high, moderate and low).

3.2.2 I_3–R_{24} rainfall index and thresholds

Rainfall-induced landslides are always triggered by either high intensity rainfall or high accumulated rainfall (Larsen and Simon, 1993; Corominas and Moya; 1999; Yu et al., 2006). In order to find out rainfall index responsible for landslides, triggering rainfall of each landslide case was analyzed according to the landslide occurrence time. It was found that there were 218 landslide cases occurred within 3 hours right after the highest rainfall intensity and 242 cases occurred within 3 hours right after the 2nd or 3rd highest rainfall intensity (i.e. induced by high rainfall intensity), accounting for nearly 49% of landslide cases gathered in this study. On the other hand, there were 481 landslide cases occurred at the time close to the end of rainfall event (i.e. induced by high accumulated rainfall), accounting for about 51% of the total cases (Table 3). Furthermore, analysis of different accumulated rainfall index showed that 24-hour accumulated rainfall has the lowest coefficient of variation (Table 4), indicating that this index was less dispersive than others and might be more suitable for establishing rainfall threshold. Based on these data and literatures (Cheung et al., 2006; Liao et al., 2010), 3-hour mean rainfall intensity (I_3) and 24-hour accumulated rainfall (R_{24}) were therefore chosen as short-term and long-term rainfall index respectively for the establishment of rainfall threshold (Fig. 4).

Finally, rainfall thresholds were decided by plotting I_3 and R_{24} rainfall index of historical landslides in the I_3–R_{24} diagram (Fig. 5). Here we used the ellipse as threshold line and the parameter a as well as b of ellipse were set according to the slope of best fit line getting from least square method. Different thresholds such as 90%, 60%, 30%, 15% were determined according to the percentage of historical cases that could be enveloped under the threshold line, e.g. the 90% threshold ($T_{90\%}$) included 90% of the historical cases and a higher threshold also indicated a more dangerous condition.

3.2.3 Landslide early warning model

Landslide early warning model in this study considered both landslide susceptibility as well as rainfall thresholds and was given warning signs by using the concept of hazard matrix. As mentioned above, LR method was applied to analyze the susceptibility of each slope unit. After that, all the slope units were categorized into high, moderate and low susceptibility level. We consequently established rainfall thresholds for each susceptibility level separately and then gave warning signs including red, orange, yellow and green according to the dangerous level.

For high susceptibility slopes (Table 5), they might be more susceptible to rainfall, hence the warning sign was set as red (extreme dangerous level) when rainfall condition exceeds the 60% threshold line; orange (high dangerous level) when rainfall condition was between the 60% and 30% threshold lines; yellow (medium dangerous level) when rainfall condition

was between the 30% and 15% thresholds lines; green (low dangerous level) when rainfall condition was lower than the 15% threshold line. For moderate susceptibility slopes (Fig. 6), the warning sign was set as red when rainfall condition exceeds the 90% threshold line; orange when rainfall condition was between the 90% and 60% threshold lines; yellow when rainfall condition was between the 60% and 30% thresholds lines; green when rainfall condition was lower than the 30% threshold line. For low susceptibility slopes, they might be less susceptible to rainfall, hence there was no red sign and the warning sign was set as orange when rainfall condition exceeds the 90% threshold line; yellow when rainfall condition was between the 90% and 60% thresholds lines; green when rainfall condition was lower than the 60% threshold line.

4 **Results and discussions**

4.1 **Landslide susceptibility analysis**

After several times of model calibration, the resultant model was obtained. The coefficients for each factor of LR were given in table 2 and the landslide susceptibility of each slope unit were also defined. In order to evaluate the quality of a predicted model, the success rate curve (SRC) and prediction rate curve (PRC) (Chung and Fabbri, 1999) were mapped and then the area under the curve (AUC) was used to describe the model's ability of distinguishing landslide and non-landslide (Yesilnacar and Topal, 2005). A higher AUC value indicated a better model. If the AUC value was 0.5, it meant that the model didn't predict the occurrence of the landslide better than a random approach. If the AUC value was close to 1.0, the capability of model that interpreting landslide was nice.

The AUC was 0.745 and 0.691 in training and validating model respectively, indicating our LR model could identify 60% of the landslides in the top 25% and 30% of the highest susceptibility areas during training and validation (Fig. 7) These results showed that the LR model was stable and nice in training as well as validation. It also represented that LR was useful in landslide susceptibility analysis.

Having enough samples were the foundation of statistic method. Due to our using slope units, the amount of samples were less than a traditional grid method, so it was not easy to establish a well-performed model compared with a grid-based landslide susceptibility model. For the sake of increasing more samples for analysis, we integrated the data from several events, but it might also brought some noises for the training. Therefore, filtering unfavorable or unsuitable samples were required.

On the other hand, for avoiding over training, it was necessary to validate the capability of model. One common method was dividing study area into sub-regions such as left and right, one for training and the other for validation (Chung and Fabbri, 2008). But it might lost training pattern in a small or particular geological region if the study area was extensive. To overcome this problem, we suggested using multi-event data in the same area for training and testing. The data used in this study were therefore divided into two parts randomly and several sets of data were tested. This would also solve the problems mentioned above.

4.2 **I_3–R_{24} rainfall threshold**

We gathered totally 941 landslide cases in this study and picked out 240 cases located in southern Taiwan, including 110 high susceptibility cases, 84 moderate susceptibility cases and 46 low susceptibility cases to establish a susceptibility-based

regional landslide early warning model. The ellipse-shaped I_3–R_{24} rainfall thresholds for 3 different landslide susceptibility slopes were shown in Table 6 and Fig. 8. For the purpose of practical use, the original threshold values of I_3 and R_{24} were rounded to 5 mm/hr and 50 mm separately as shown in the parentheses in Table 6. It could be found that the threshold values gradually decreased as the susceptibility of slope decreased for the same threshold (e.g. $T_{90\%}$) and the threshold values also gradually decreased as the susceptibility of slope increased for the same warning sign. This results showed that establishing rainfall thresholds according to different landslide susceptibility and then set warning signs by adopting the concept of hazard matrix could not only provide differentiated thresholds but also avoid an overestimate or underestimate of the thresholds for slopes. In addition, Table 7. showed the warning signs and the corresponding dangerous levels as well as suggested action for residents around the warning slope. During a yellow sign, residents should pay attention to whether there are further announcements or not and ready for an evacuation if the sign turns to orange. While an orange sign is issued, residents should evacuate as quickly as possible because landslides are prone to occur according to the validations shown in the next section. Lastly, when the warning sign goes to red, forced evacuation might need to prevent residents from getting injured.

4.3 Validation of landslide early warning model

We validated our model with two kinds of data: (1) three disastrous shallow landslide cases in 2016 and the occurrence time provided by witnesses; (2) landslide inventory of two historical typhoon events and the occurrence time reported by newspapers.

For the first one, it showed that all the disastrous landslide cases could be warned with orange or red sign in advance before landslide occurred according to the rainfall snake line in the I_3–R_{24} diagram (Fig. 9.; Table 8.).

Shihwen landslide occurred on a low susceptibility slope. Form the rainfall histogram and I_3–R_{24} diagram (Fig. 9(a)), we knew that the occurrence time was quite close to the end of rainfall event and the I_3 was only 2.3 mm/hr while the R_{24} was 507.5 mm, indicating that accumulated rainfall might be the principal cause of this case. Rainfall snake line showed that the warning sign turned to yellow at 10:00, 14th and soon turned to orange at 11:00 during the downpour; then it was a little bit let up for several hours and the warning sign turned back to yellow. However, when it rained again, the warning sign also turned to orange again at 18:00 as well as 23:00 and finally the landslide occurred at 05:00, 15th.

Zhongmin landslide occurred on a high susceptibility slope. Form the rainfall histogram and I_3–R_{24} diagram (Fig. 9(b)), it could be found that the occurrence time was also quite close to the end of rainfall event and the I_3 was 8.3 mm/hr while the R_{24} was 479 mm. The high rainfall intensity (74 mm/hr at 04:00, 28th, September) as well as accumulated rainfall might both result in this landslide. Rainfall snake line showed that the warning sign turned to yellow and then quickly turned to orange and red at 04:00, 28th during high intensity rainfall mentioned above. After that, although it let up soon, the landslide finally occurred 6 hours later at 10:00, 28th during the orange sign.

Houcuo landslide also occurred on a low susceptibility slope. Form the rainfall histogram and I_3–R_{24} diagram (Fig. 9(c)), we knew that the occurrence time was almost near the highest rainfall intensity in the rainfall event and the I_3 was 24.3 mm/hr while the R_{24} was 291.3 mm, indicating that high rainfall intensity might be responsible for this case. Due to this intensity, rainfall snake line showed that the warning sign turned from green to yellow and orange in just one hour during 03:00 ~ 04:00, 28th, the landslide also occurred around 03:30, 28th.

For the second one, we applied Kriging method to interpolate special rainfall data and analyzed the warning sign of each slope unit hour by hour. It showed that the hitting ratio in two historical typhoon events were all high enough according to the accumulative warning numbers relative to the numbers of landslide slopes (Fig. 10.; Table 9.).

During Typhoon Mindulle in 2004, there were 10,911 slope units once landslide, including 5,129 high susceptibility slopes, 2,750 moderate susceptibility slopes and 3,032 low susceptibility slopes. According to the reports in newspapers, several landslides occurred at 10:00 and 15:00 ~ 16:00, 2nd, July, 2004; however, most of the landslides occurred during 06:00 ~ 13:00, 3rd, July, 2004 (blue dashed box in Fig. 10(a)). From the warning history (Fig. 10(a)), it could be found that the peak number of orange and red signs fitted the reported occurrence time quite well. Besides, there were 8,283 slope units ever be warned as orange sign, which is the sign for evacuation, during the whole event, accounting for 75.9% of the slope units once landslide.

Typhoon Haitang in 2005 was another event of concern. There were 10,804 slope units once landslide, including 2,592 high susceptibility slopes, 2,355 moderate susceptibility slopes and 5,857 low susceptibility slopes. According to the reports in newspapers, landslides occurred from 05:00, 19th to 06:00, 20th, July, 2005 (blue dashed box in Fig. 10(b)). From the warning history (Fig. 10(b)), it could be found that landslide occurred right after the number of orange and red signs increased sharply and the peak number of orange and red signs also fitted the reported occurrence time quite well. On the other hand, there were 10,245 slope units ever be warned as orange sign during the whole event, accounting for 94.8% of the slope units once landslide. These results revealed that our model could provide valuable information for evacuation and disaster prevention.

5 Conclusions

In order to verify if the difference in susceptibility might lead to a difference in warning threshold, we divided slope units into three susceptibility levels (high, moderate, low) based on the results of Logistic Regression (LR) and established their rainfall thresholds separately in this study. I_3–R_{24} rainfall index, a combination of short-term as well as long-term rainfall index, were used for the establishment of rainfall thresholds. After that, three warning signs including yellow (advisory), orange (watch) and red (warning) were set by adopting the concept of hazard matrix. It was found that the warning thresholds were different for each susceptibility level and gradually decreased as the susceptibility of slope increased. Validations from three disastrous shallow landslides in 2016 showed that they can be warned in advance before landslide occurred and validations from two serious historical typhoon events also showed that the hitting ratio of our early waring model were 75.9% and 94.8% respectively. It could be concluded that classifying landslide susceptibility and establishing rainfall thresholds separately might be able to provide differentiated warning thresholds for different susceptibility levels.

Acknowledgements

The authors would like to thank the Central Geological Survey, Taiwan, for supporting this research financially and providing helpful comments on the research.

References

1. Ayalew, L.: The effect of seasonal rainfall on landslides in the highlands of Ethiopia, B Eng Geol Environ, 58(1), 9–19, 1999.
2. Bell, F. G., and Maud, R. R.: Landslides associated with the colluvial soils overlying the Natal Group in the greater Durban region of Natal, South Africa, Environ Geol, 39(9), 1029–1038, 2000.
3. Brunetti, M. T., Peruccacci, S., Rossi, M., Luciani, S., Valigi, D., and Guzzetti, F.: Rainfall thresholds for the possible occurrence of landslides in Italy, Nat Hazard Earth Sys, 10(3), 447–458, 2010.
4. Caine, N.: The rainfall intensity-duration control of shallow landslides and debris flows, Geogr Ann A, 62, 23–27, 1980.
5. Carrara, A.: Drainage and divide networks derived from high-fidelity digital terrain models, Quantitative Analysis of Mineral and Energy Resources, in: Quantitative analysis of mineral and energy resources, Springer, Dordrech, 581–597, 1988.
6. Carrara, A., and Guzzetti, F.: GIS Technology in Mapping Landslide Hazard, in: Geographical information systems in assessing natural hazards, Springer, Netherlands, 135–175, 1995.
7. Carrara, A., Cardinali, M., Detti, R., Guzzetti, F., Pasqui, V., and Reichenbach, P.: GIS Techniques and statistical models in evaluating landslide hazard, Earth Surf Proc Land, 16(5), 427–445, 1991.
8. Cheung, S. P. Y., Wong, M. C., and Yeung, L. H. Y.: Application of rainstorm nowcast to real-time warning of landslide hazards in Hong Kong, in: WMO PWS Workshop on Warnings of Real-Time Hazards by Using Nowcasting Technology, Sydney, Australia, 1–21, 2006.
9. Chung, C. J., and Fabbri, A. G.: Predicting landslides for risk analysis - spatial models tested by a cross-validation technique. Geomorphology, 94(3), 438–452, 2008.
10. Corominas, J., and Moya, J.: Reconstructing recent landslide activity in relation to rainfall in the Llobregat River basin, Eastern Pyrenees, Spain. Geomorphology, 30(1), 79–93, 1999.
11. Evans, S. G., Guthrie, R. H., Roberts, N. J., and Bishop, N. F.: The disastrous 17 February 2006 rockslide-debris avalanche on Leyte Island, Philippines: a catastrophic landslide in tropical mountain terrain, Nat Hazard Earth Sys, 7(1), 89–101, 2007.
12. Fan, X., Xu, Q., Scaringi, G., Dai, L., Li, W., Dong, X., Zhu, X., Pei, X., Dai, K., and Havenith, H. B.: Failure mechanism and kinematics of the deadly June 24th 2017 Xinmo landslide, Maoxian, Sichuan, China, Landslides, 14(6), 2129–2146, 2017.
13. Franklin, J. A.: Safety and Enconomy in Tunneling, in: Proc. 10th Can. Rock Mech. Symp, Queens University, Kingston, Canada, 325–341, 1975.
14. Gariano, S. L., Brunetti, M. T., Iovine, G., Melillo, M., Peruccacci, S., Terranova, Terranova, O., Vennari, C., and Guzzetti, F.: Calibration and validation of rainfall thresholds for shallow landslide forecasting in Sicily, southern Italy, Geomorphology, 228, 653–665, 2015.
15. Gorsevski, P. V., and Jankowski, P.: An optimized solution of multicriteria evaluation analysis of landslide susceptibility using fuzzy sets and Kalman filter, Comput Geosci, 36(8), 1005–1020, 2010.
16. Guzzetti, F., Carrara, A., Cardinali, M., and Reichenbach, P.: Landslide hazard evaluation: a review of current techniques and their application in a multi-scale study, Central Italy, Geomorphology, 31(1), 181–216, 1999.
17. Guzzetti, F., Peruccacci, S., Rossi, M., and Stark, C. P.: The rainfall intensity-duration control of shallow landslides and debris flows: an update, Landslides, 5(1), 3–17, 2008.
18. Guzzetti, F., Peruccacci, S., Rossi, M., and Stark, C. P.: Rainfall thresholds for the initiation of landslides in central and

southern Europe. Meteorol Atmos Phys, 98(3-4), 239–267, 2007.

19. Guzzetti, F., Mondini, A. C., Cardinali, M., Fiorucci, F., Santangelo, M., and Chang, K. T.: Landslide inventory maps: New tools for an old problem. Earth-Sci Rev, 112(1), 42–66, 2012.
20. Hong, Y., Hiura, H., Shino, K., Sassa, K., Suemine, A., Fukuoka, H. and Wang, G.: The influence of intense rainfall on the activity of large-scale crystalline schist landslides in Shikoku Island, Japan, Landslides, 2(2), 97–105, 2005.
21. Hong, Y., and Adler, R. F.: Predicting global landslide spatiotemporal distribution: integrating landslide susceptibility zoning techniques and real-time satellite rainfall estimates, Int J Sediment Res, 23(3), 249–257, 2008.
22. Iverson, R. M., George, D. L., Allstadt, K., Reid, M. E., Collins, B. D., Vallance, J. W., Schilling, S. P., Godt, J. W., Cannon, C. M., Magirl, C. S., Baum, R. L., Coe, J. A., Schulz, W. H., and Bower, J. B.: Landslide mobility and hazards: implications of the 2014 Oso disaster, Earth Planet Sc Lett , 412, 197–208, 2015.
23. Kim, D., Im, S., Lee, S. H., Hong, Y., and Cha, K. S.: Predicting the rainfall-triggered landslides in a forested mountain region using TRIGRS model, J Mt Sci, 7(1), 83–91, 2010.
24. Larsen, M. C., and Simon, A.: A rainfall intensity-duration threshold for landslides in a humid-tropical environment, Puerto Rico, Geografiska Annaler, Series A, Phys Geogr, 13–23, 1993.
25. Lee, C. T.: Statistical Seismic Landslide Hazard Analysis: An Example from Taiwan, Eng Geol, 182, 201–212, 2014.
26. Lee, C. T., Huang, C. C., Lee, J. F., Pan, K. L., Lin, M. L., and Dong, J. J.: Statistical Approach to Earthquake-Induced Landslide Susceptibility. Eng Geol, 100(1-2), 43–58, 2008a.
27. Lee, C. T., Huang, C. C., Lee, J. F., Pan, K. L., Lin, M. L., and Dong, J. J.: Statistical approach to storm event-induced landslide susceptibility, Nat Hazard Earth Sys, 8(4), 941–960, 2008b.
28. Lee, C. T., Huang, C. C., Lee, J. F., Pan, K. L., Lin, M. L., Liao, C. W., Lin, P. S., Lin, Y. S., Chang, C. W.: Landslide susceptibility analyses based on three different triggering events and result comparison, in: Proceeding of International Symposium on Landslide and Debris Flow Hazard Assessment, 6, 1–18, 2004.
29. Lee, S., Won, J. S., Jeon, S. W., Park, I., and Lee, M. J.: Spatial landslide hazard prediction using rainfall probability and a logistic regression model, Math Geosci, 47(5), 565–589, 2015.
30. Lee M. J., Choi J. W., Oh H. J., Won J. S., Park I. and Lee, S.: Ensemble based landslide susceptibility maps in Jinbu area, Korea, Environ Earth Sci, 67(1), 23-37, 2012.
31. Liao, Z., Hong, Y., Wang, J., Fukuoka, H., Sassa, K., Karnawati, D., and Fathani, F.: Prototyping an experimental early warning system for rainfall-induced landslides in Indonesia using satellite remote sensing and geospatial datasets, Landslides, 7(3), 317–324, 2010.
32. Luo, W., and Liu, C. C.: Innovative landslide susceptibility mapping supported by geomorphon and geographical detector methods, Landslides, online first, 2017
33. Marjanović, M., Kovačević, M., Bajat, B., and Voženílek, V.: Landslide susceptibility assessment using SVM machine learning algorithm, Eng Geol, 123(3), 225–234, 2011.
34. Martelloni, G., Segoni, S., Fanti, R., and Catani, F.: Rainfall thresholds for the forecasting of landslide occurrence at regional scale, Landslides, 9(4), 485–495, 2011.
35. Montgomery, D. R., and Dietrich, W.E.: A physical-based model for the topographic control on shallow landsliding, Water Resour Res, 30(4), 1153–1171, 1994.
36. Osanai, N., Shimizu, T., Kuramoto, K., Kojima, S., and Noro, T.: Japanese early-warning for debris flows and slope failures using rainfall indices with Radial Basis Function Network, Landslides, 7(3), 325–338, 2010.
37. Petley, D.: Global patterns of loss of life from landslides, Geology, 40(10), 927–930, 2012.
38. Peruccacci, S., Brunetti, M. T., Gariano, S. L., Melillo, M., Rossi, M., and Guzzetti, F.: Rainfall thresholds for possible

landslide occurrence in Italy, Geomorphology, 290, 39–57, 2017.

39. Pradhan, A. M. S., Kang, H. S., Lee, J. S., and Kim, Y. T.: An ensemble landslide hazard model incorporating rainfall threshold for Mt. Umyeon, South Korea, B Eng Geol Environ, online first, 2017.
40. Rosi, A., Lagomarsino, D., Rossi, G., Segoni, S., Battistini, A., and Casagli, N.: Updating EWS rainfall thresholds for the triggering of landslides. Nat Hazards, 78(1), 297–308, 2015.
41. Rossi, M., Luciani, S., Valigi, D., Kirschbaum, D., Brunetti, M. T., Peruccacci, S., and Guzzetti, F.: Statistical approaches for the definition of landslide rainfall thresholds and their uncertainty using rain gauge and satellite data, Geomorphology, 285, 16–27, 2017.
42. Samia, J., Temme, A., Bregt, A., Wallinga, J., Guzzetti, F., Ardizzone, F., and Rossi, M.: Do landslides follow landslides? Insights in path dependency from a multi-temporal landslide inventory, Landslides, 14(2), 547–558, 2017.
43. Sassa, K., Tsuchiya, S., Fukuoka, H., Mikos, M., and Doan, L.: Landslides: review of achievements in the second 5-year period (2009–2013), Landslides, 12(2), 213–223, 2015.
44. Schlögel, R., Marchesini, I., Alvioli, M., Reichenbach, P., Rossi, M., and Malet, J. P.: Optimizing landslide susceptibility zonation: Effects of DEM spatial resolution and slope unit delineation on logistic regression models, Geomorphology, online first, 2017.
45. Segoni, S., Rosi, A., Rossi, G., Catani, F., and Casagli, N.: Analysing the relationship between rainfalls and landslides to define a mosaic of triggering thresholds for regional-scale warning systems, Nat Hazard Earth Sys, 14(9), 2637, 2014.
46. Segoni, S., Lagomarsino, D., Fanti, R., Moretti, S., and Casagli, N.: Integration of rainfall thresholds and susceptibility maps in the Emilia Romagna (Italy) regional-scale landslide warning system, Landslides, 12(4), 773–785, 2015.
47. Song, K. Y., Oh, H. J., Choi, J., Park, I., Lee, C., and Lee, S.: Prediction of landslide using ASTER imagery and data mining models, Adv Space Res, 49, 978–993, 2012.
48. Terlien, M. T.: The determination of statistical and deterministic hydrological landslide-triggering thresholds, Eng Geol, 35(2-3), 124–130, 1998.
49. Tsou, C. Y., Feng, Z. Y., and Chigira, M.: Catastrophic landslide induced by typhoon Morakot, Shiaolin, Taiwan, Geomorphology, 127(3), 166–178, 2011.
50. Turkington, T., Ettema, J., van Westen, C. J. and Breinl, K.: Empirical atmospheric thresholds for debris flows and flash floods in the Southern French Alps, Nat Hazard Earth Sys, 14, 1517–1530, 2014.
51. Valenzuela, P., Domínguez-Cuesta, M. J., García, M. A. M., and Jiménez-Sánchez, M.: A spatio-temporal landslide inventory for the NW of Spain: BAPA database, Geomorphology, 293, 11–23, 2017.
52. Van Westen, C. J., and Terlien, M. T. J.: An approach towards deterministic landslide hazard analysis in GIS: A case study from Manizales (Colombia), Earth Surf Proc Land, 21, 853–868, 1996.
53. Van Westen, C. J., Rengers, N., and Soeters, R.: Use of geomorphological information in indirect landslide susceptibility assessment, Nat Hazards, 30(3), 399–419, 2003.
54. Vessia, G., Parise, M., Brunetti, M. T., Peruccacci, S., Rossi, M., Vennari, C. and Guzzetti, F.: Automated reconstruction of rainfall events responsible for shallow landslides. Nat Hazard Earth Sys, 14(9), 2399–2408, 2014.
55. Wang, F., Wu, Y. H., Yang, H., Tanida, Y., and Kamei, A.: Preliminary investigation of the 20 August 2014 debris flows triggered by a severe rainstorm in Hiroshima City, Japan, Geoenvironmental Disasters, 2(1), 17, 2015.
56. Wilson, J. P. and Gallant, J. C.: Terrain analysis: principles and applications, John Wiley & Sons, Inc., 2000.
57. Xie, M., Esaki, T. and Zhou, G.: GIS-based probabilistic mapping of landslide zazard using a three-dimensional deterministic model, Nat Hazards, 33(2), 265–282, 2004.
58. Yang, S. R.: Assessment of Rainfall-Induced Landslide Susceptibility Using GIS-Based Slope Unit Approach, J Perform

Constr Fac, 31(4), 04017026, 2017.

59. Yeon, Y. K., Han, J. G., and Ryu, K. H.: Landslide susceptibility mapping in Injae, Korea, using a decision tree, Eng Geol, 116(3), 274–283, 2010.
60. Yesilnacar, E., and Topal, T.: Landslide susceptibility mapping : A comparison of logistic regression and neural networks methods in a medium scale study, Hendek region (Turkey), Eng Geol, 79(3), 251–266, 2005.
61. Yilmaz I.: Comparison of landslide susceptibility mapping methodologies for Koyulhisar, Turkey: conditional probability, logistic regression, artificial neural networks, and support vector machine, Environ Earth Sci 61(4), 821-836, 2010.
62. Yu, F. C., Chen, T. C., Lin, M. L., Chen, C. Y., and Yu, W. H.: Landslides and rainfall characteristics analysis in Taipei City during the Typhoon Nari event, Nat hazards, 37(1), 153–167, 2006.
63. Zhou, W., Tang, C., Van Asch, T. W., and Zhou, C.: Rainfall-triggering response patterns of post-seismic debris flows in the Wenchuan earthquake area, Nat. Hazards, 70(2), 1417–1435, 2014.

Nat. Hazards Earth Syst. Sci. Discuss., https://doi.org/10.5194/nhess-2017-428
Manuscript under review for journal Nat. Hazards Earth Syst. Sci.
Discussion started: 19 December 2017

Natural Hazards and Earth System Sciences
Discussions

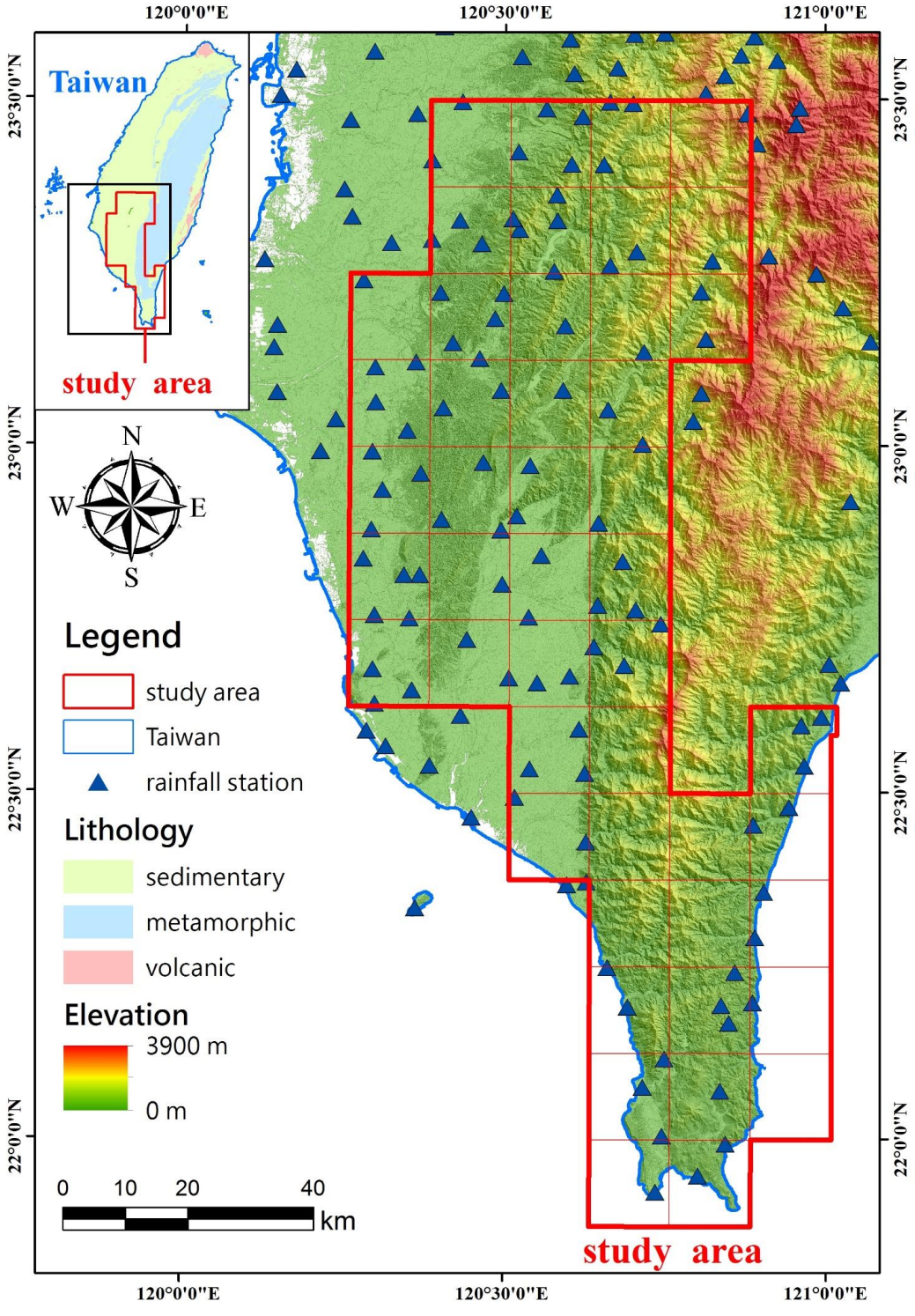

Figure 1: Geomorphological and geological settings of study area.

Nat. Hazards Earth Syst. Sci. Discuss., https://doi.org/10.5194/nhess-2017-428
Manuscript under review for journal Nat. Hazards Earth Syst. Sci.
Discussion started: 19 December 2017

Natural Hazards and Earth System Sciences
Discussions

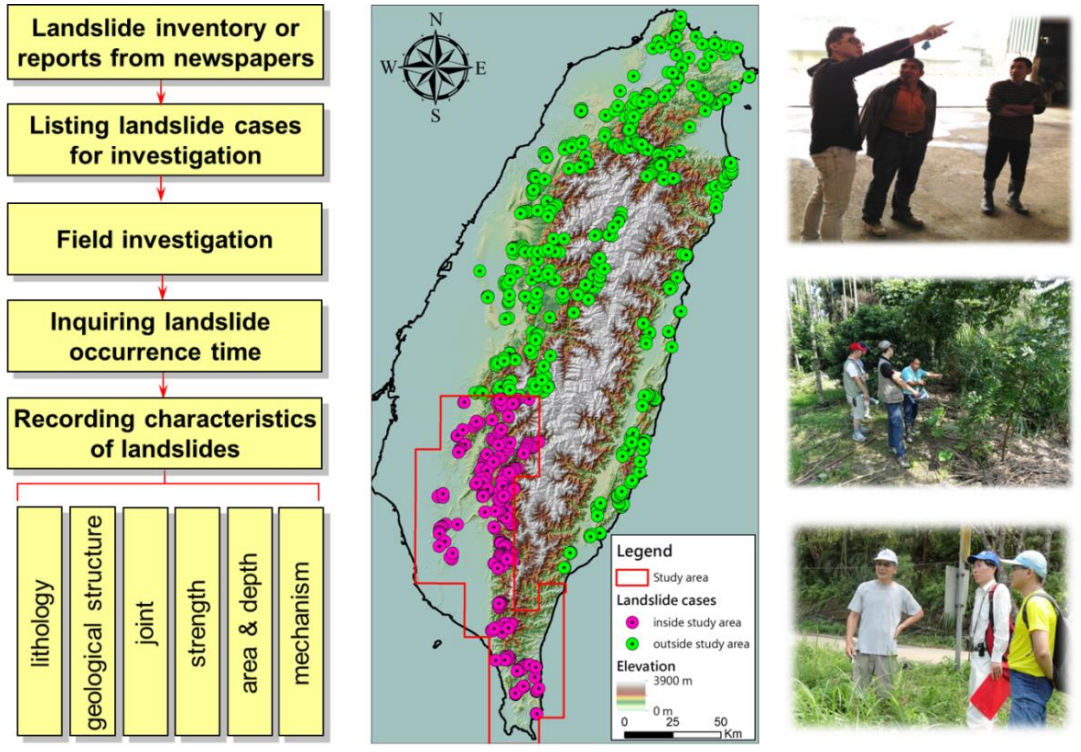

Figure 2: Flowchart of landslide occurrence time gathering during field investigation (left), location of landslide cases with the occurrence time used in this study (middle) and the pictures of inquiring residents (right).

5

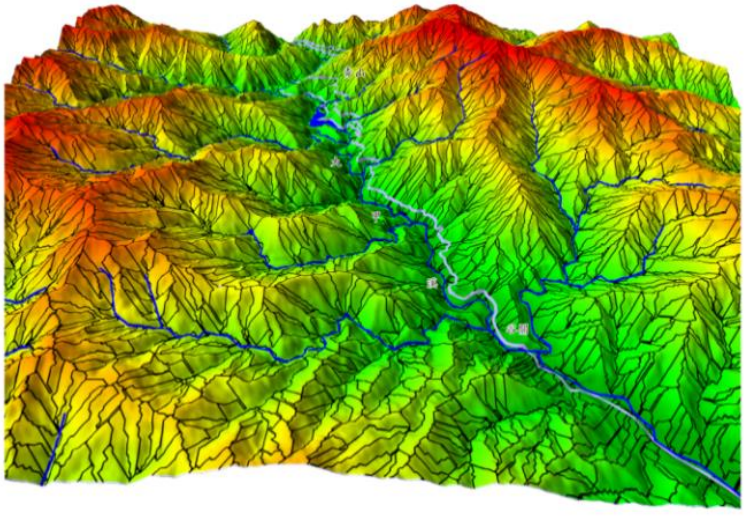

Figure 3: A display of Slope unit.

Nat. Hazards Earth Syst. Sci. Discuss., https://doi.org/10.5194/nhess-2017-428
Manuscript under review for journal Nat. Hazards Earth Syst. Sci.
Discussion started: 19 December 2017

Natural Hazards and Earth System Sciences
Discussions

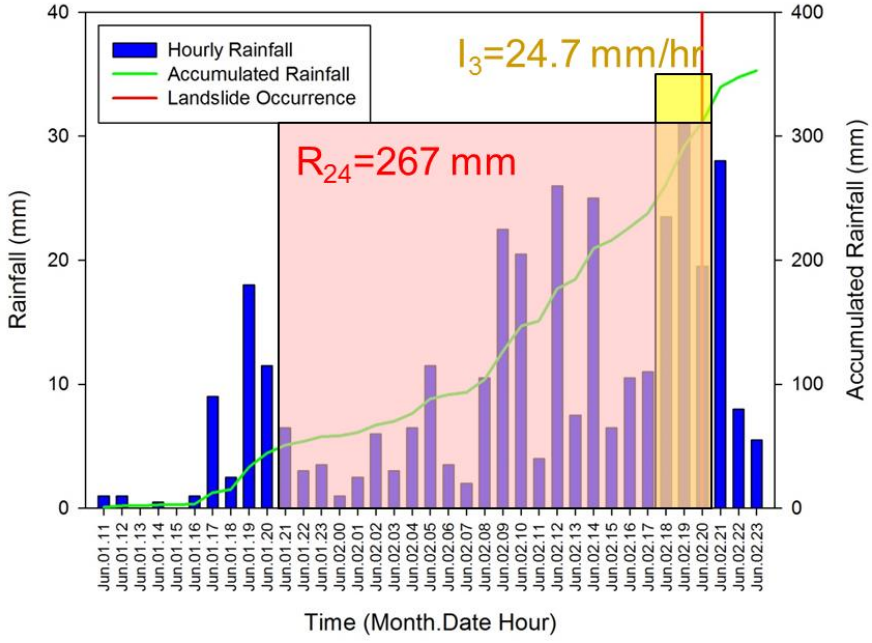

Figure 4: 3-hour mean rainfall intensity (I_3) and 24-hour accumulated rainfall (R_{24}) were used as short-term and long-term rainfall index.

5

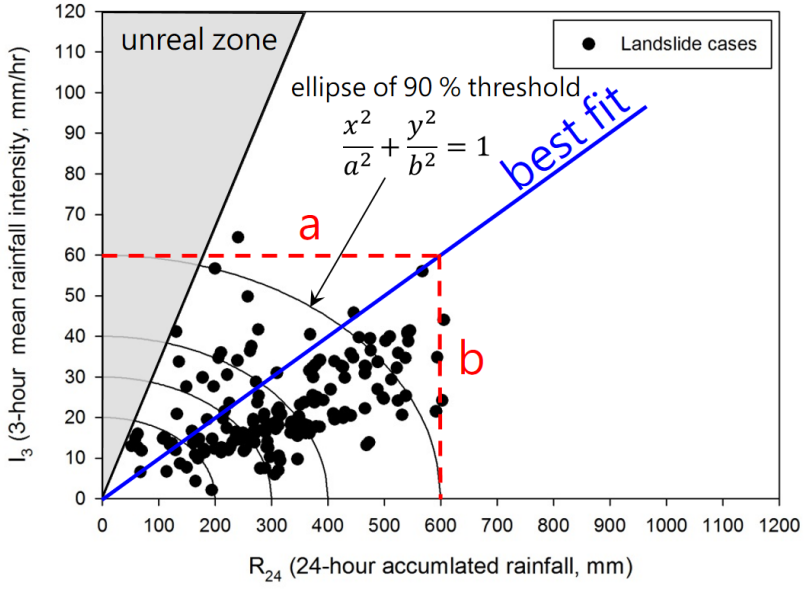

Figure 5: Establishment of I_3–R_{24} rainfall thresholds for shallow landslides.

Nat. Hazards Earth Syst. Sci. Discuss., https://doi.org/10.5194/nhess-2017-428
Manuscript under review for journal Nat. Hazards Earth Syst. Sci.
Discussion started: 19 December 2017

Natural Hazards and Earth System Sciences
Discussions

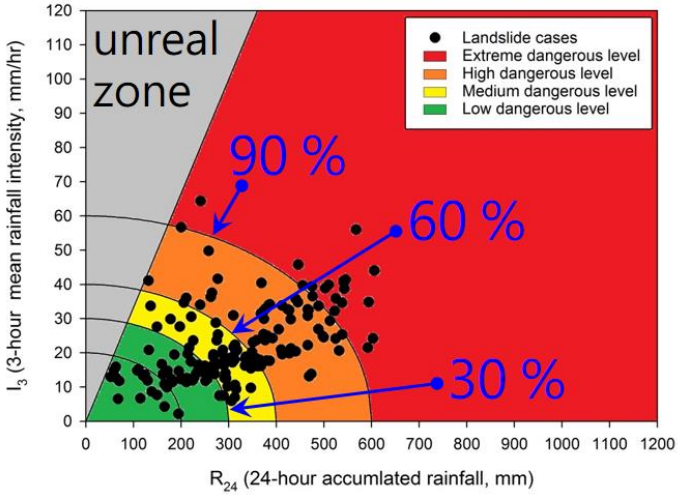

Figure 6: I_3–R_{24} landslide early warning model and the warning sign (moderate susceptibility as example)

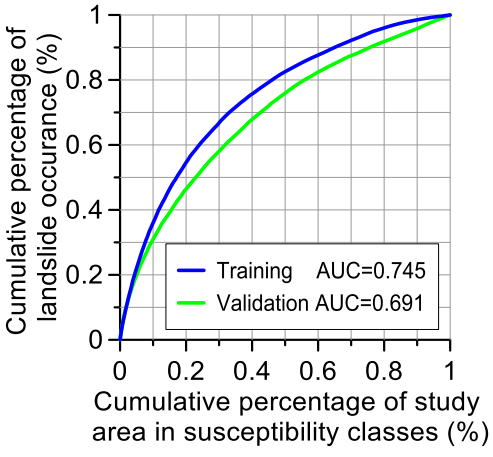

Figure 7: Result of training and validation

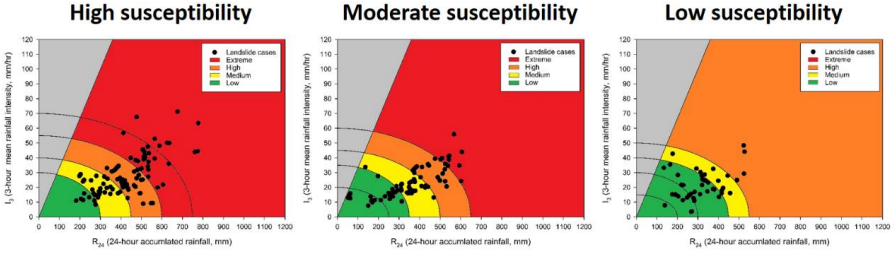

Figure 8: I_3–R_{24} rainfall thresholds for southern Taiwan

Nat. Hazards Earth Syst. Sci. Discuss., https://doi.org/10.5194/nhess-2017-428
Manuscript under review for journal Nat. Hazards Earth Syst. Sci.
Discussion started: 19 December 2017

Natural Hazards and Earth System Sciences
Discussions

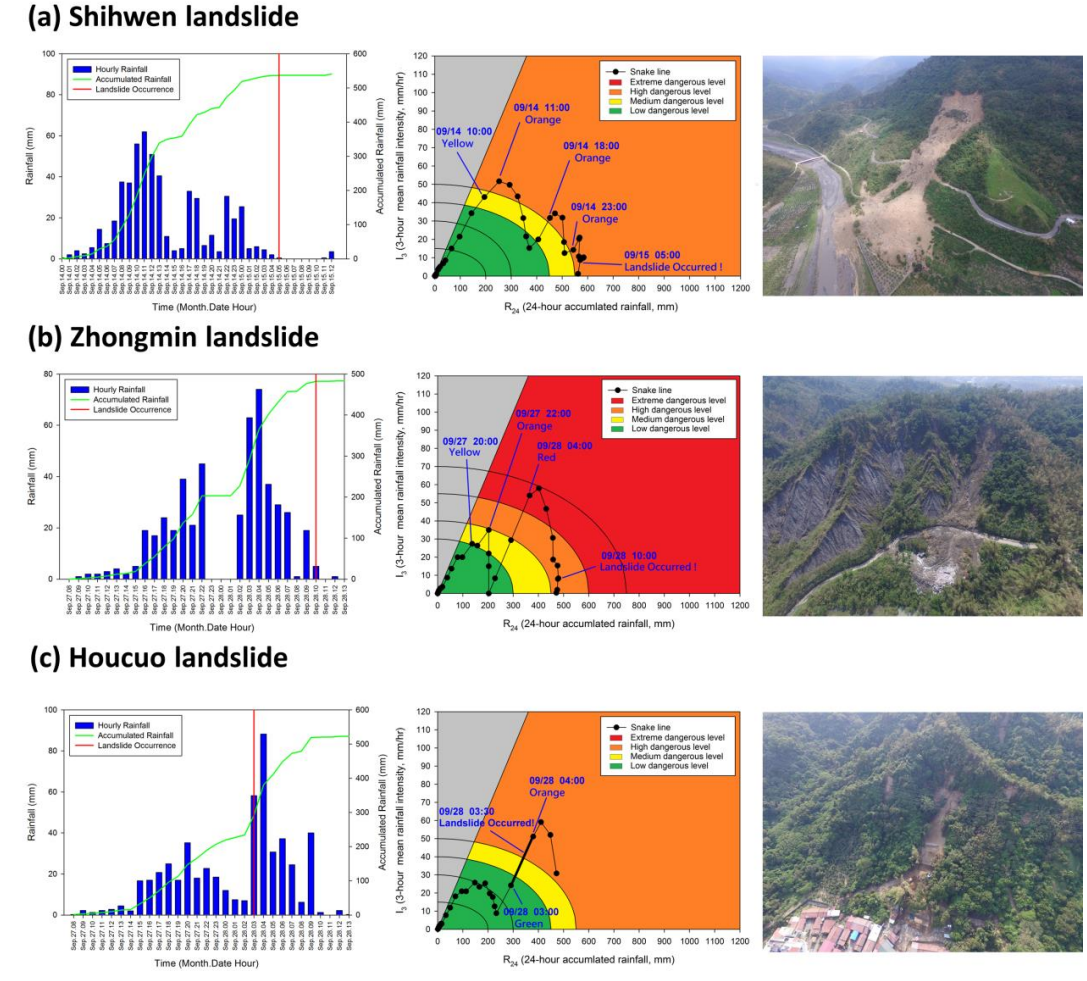

Figure 9: Disastrous landslide cases in 2016 and their rainfall histogram as well as snake line in the I_3–R_{24} diagram.

Nat. Hazards Earth Syst. Sci. Discuss., https://doi.org/10.5194/nhess-2017-428
Manuscript under review for journal Nat. Hazards Earth Syst. Sci.
Discussion started: 19 December 2017

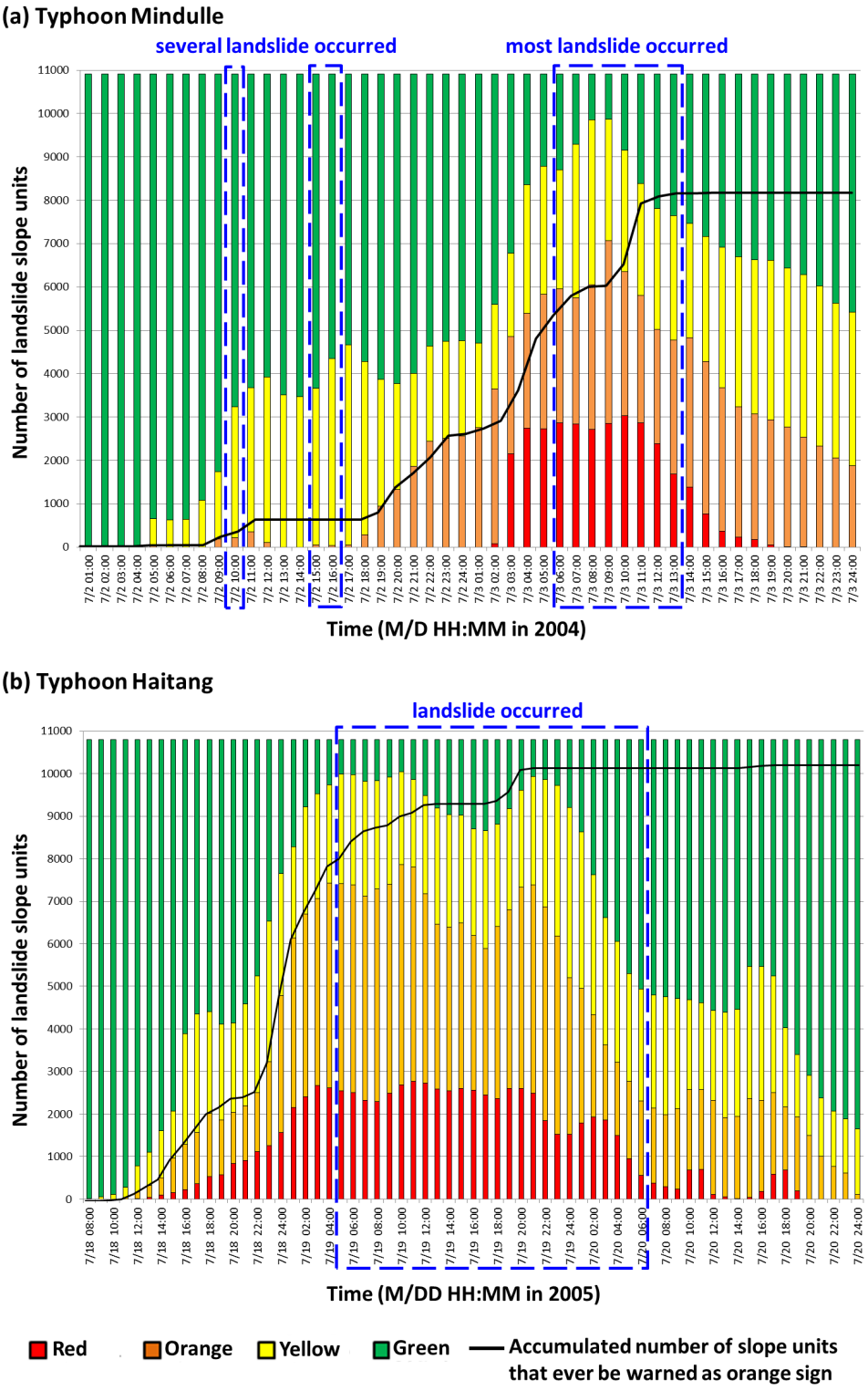

Figure 10: Warning history of (a) Typhoon Mindulle and (b) Typhoon Haitang

Nat. Hazards Earth Syst. Sci. Discuss., https://doi.org/10.5194/nhess-2017-428
Manuscript under review for journal Nat. Hazards Earth Syst. Sci.
Discussion started: 19 December 2017

Natural Hazards and Earth System Sciences
Discussions

Table 1: The multi-year landslide inventory

Year	Event
2004	Before Typhoon Mindulle
2004	After Typhoon Mindulle
2005	After Typhoon Haitang
2006	After 0609 Torrential rainfall
2007	After Typhoon Sepat
2008	After Typhoon Sinlaku
2009	After Typhoon Morakot

Table 2: Factor items and logistic function coefficient

Code	Factor item	coefficient
L_{01}	RMSSC I	-
L_{02}	RMSSC II	-
L_{03}	RMSSC III	-0.874
L_{04}	RMSSC IV	-0.099
L_{05}	RMSSC V	0.314
L_{06}	RMSSC VI	-0.384
L_{07}	RMSSC VII	-
F_{01}	dip slope	0.207
F_{02}	average slope	0.265
F_{03}	variance of slope	0.098
F_{04}	ratio of steep slope	0.344
F_{05}	average curvature	0.016
F_{06}	variance of curvature	0.161
F_{07}	fold density	0.013
F_{08}	average wetness	0.061
F_{09}	I_3	-0.817
F_{10}	R_{24}	0.665
C	Constant	0.057

Table 3: Type and the proportion of landslide occurrence time.

type of landslide occurrence time	amount (percentage)
Type A: within 3 hours right after the highest rainfall intensity (landslide induced by high rainfall intensity)	218 (23%)
Type B: within 3 hours right after the 2nd or 3rd highest rainfall intensity (landslide induced by high rainfall intensity)	242 (26%)
Type C: near the end of rainfall event (landslide induced by high accumulated rainfall)	481 (51%)
total	941 (100%)

Nat. Hazards Earth Syst. Sci. Discuss., https://doi.org/10.5194/nhess-2017-428
Manuscript under review for journal Nat. Hazards Earth Syst. Sci.
Discussion started: 19 December 2017

Natural Hazards and Earth System Sciences
Discussions

Table 4: Coefficient of variation of different accumulated rainfall index

Accumulated rainfall Indexes	Coefficient of Variation
6-hour accumulated rainfall (R_6)	0.68
12-hour accumulated rainfall (R_{12})	0.47
24-hour accumulated rainfall (R_{24})	0.38
48-hour accumulated rainfall (R_{48})	0.41
72-hour accumulated rainfall (R_{72})	0.45

Table 5: Landslide early warning model and the warning sign considering both landslide susceptibility and rainfall thresholds

		Rainfall threshold (T)			
		$T_{90\%}$	$T_{60\%}$	$T_{30\%}$	$T_{15\%}$
Landslide susceptibility	High susceptibility	Extreme dangerous level	Extreme dangerous level	High dangerous level	Medium dangerous level
	Moderate susceptibility	Extreme dangerous level	High dangerous level	Medium dangerous level	Low dangerous level
	Low susceptibility	High dangerous level	Medium dangerous level	Low dangerous level	Low dangerous level

Table 6: Rainfall thresholds for southern Taiwan. I_3 was rounded to 5 mm/hr, R_{24} was rounded to 50 mm and parentheses referred to the original value.

		Rainfall threshold (T)							
		$T_{90\%}$		$T_{60\%}$		$T_{30\%}$		$T_{15\%}$	
		I_3	R_{24}	I_3	R_{24}	I_3	R_{24}	I_3	R_{24}
Landslide susceptibility	High susceptibility	70 (68)	750 (745)	55 (56)	600 (610)	40 (40)	450 (438)	30 (27)	300 (291)
	Moderate susceptibility	60 (61)	650 (657)	45 (46)	500 (498)	35 (34)	350 (368)	20 (22)	250 (236)
	Low susceptibility	50 (50)	550 (539)	40 (40)	450 (430)	30 (29)	300 (316)	15 (15)	200 (167)

Table 7: Warning signs and the corresponding dangerous levels as well as suggested actions.

Warning sign	Dangerous level	Suggested action
Green	Low	-
Yellow	Medium	Notice announcements
Orange	High	Evacuation
Red	Extreme	Forced evacuation

Nat. Hazards Earth Syst. Sci. Discuss., https://doi.org/10.5194/nhess-2017-428
Manuscript under review for journal Nat. Hazards Earth Syst. Sci.
Discussion started: 19 December 2017

Natural Hazards and Earth System Sciences Discussions

Table 8: Disastrous landslide cases in 2016 and the validation results. These landslide cases could all be warned in advance or just on time.

Landslide susceptibility	Lithology	Landslide area	Warning sign & warning time	Occurrence of Landslide	Early (+) Late (-)
Shihwen landslide (Shihwen villiage, Chunri Township, Pingtung County)					
Low	Weathered sandstone	61,500 m^2	Orange, firstly at 11:00, 14th September, 2016	05:00, 15th September, 2016	+18 hours
Zhongmin landslide (Zhongmin Rd., Yanchao District, Kaohsiung City)					
High	Mudstone interbedded with thin sandstone	3,500 m^2	Orange and red, 04:00, 28th September, 2016	10:00, 28th September, 2016	+ 6 hours
Houcuo landslide (Houcuo Ln., Qishan District, Kaohsiung City)					
Low	Conglomerate	4,000 m^2	Orange, 03:00 ~ 04:00, 28th September, 2016	03:30, 28th September, 2016	0 hour

Table 9: Validation and the hitting ratio of Typhoon Mindulle and Haitang

Typhoon event (year)	Landslide occurrence time reported by newspapers	Number of landslide slope units (Number of high; moderate; low susceptibility slope units)	Number of slope units ever be warned as orange sign	Hitting Ratio
Mindulle (2004)	Mainly 06:00 ~ 13:00, 3rd, July	10,911 (5,129; 2,750; 3,032)	8,283	75.9%
Haitang (2005)	From 05:00, 19th to 06:00, 20th, July	10,804 (2,592; 2,355; 5,857)	10,245	94.8%